

Equation of State of *hcp* Fe-C-Si Alloys and the Effect of C Incorporation Mechanism on the Density of *hcp* Fe Alloys at 300 K

M. G. Pamato^{1,2} , Y. Li¹ , D. Antonangeli³ , F. Miozzi^{3,4} , G. Morard^{3,5}, I. G. Wood¹ , L. Vočadlo¹, J. P. Brodholt¹ , and M. Mezouar⁶

¹Department of Earth Sciences, University College London, London, UK, ²Department of Geosciences, University of Padova, Padova, Italy, ³Sorbonne Université, Muséum National d'Histoire Naturelle, UMR CNRS 7590, Institut de Minéralogie, de Physique des Matériaux et de Cosmochimie, IMPMC, Paris, France, ⁴Dipartimento di Scienze della Terra, Università degli Studi di Milano, Milan, Italy, ⁵Université Grenoble Alpes, Université Savoie Mont Blanc, CNRS, IRD, IFSTTAR, ISTerre, Grenoble, France, ⁶European Synchrotron Radiation Facility, Grenoble, France

Key Points:

- Synchrotron X-ray diffraction and density functional theory calculations were performed on *hcp* Fe-C-Si alloy with 4 at% C and 3 at% Si
- Different incorporation mechanisms were examined, and the *hcp* Fe-C-Si alloy sample takes the interstitial form
- Assuming a wrong incorporation mechanism leads to incorrect density determination and a more enhanced density contrast between the alloy and pure Fe

Supporting Information:

- Supporting Information S1

Correspondence to:

M. G. Pamato,
martha.pamato@unipd.it

Citation:

Pamato, M. G., Li, Y., Antonangeli, D., Miozzi, F., Morard, G., Wood, I. G., et al. (2020). Equation of state of *hcp* Fe-C-Si alloys and the effect of C incorporation mechanism on the density of *hcp* Fe alloys at 300 K. *Journal of Geophysical Research: Solid Earth*, 125, e2020JB020159. <https://doi.org/10.1029/2020JB020159>

Received 10 MAY 2020

Accepted 15 OCT 2020

Accepted article online 4 NOV 2020

Abstract Si and C are cosmochemically abundant elements soluble in *hcp* Fe under pressure and temperature and could therefore be present in the Earth's inner core. While recent ab initio calculations suggest that the observed inner core density and velocities could be matched by an Fe-C-Si alloy, the combined effect of these two elements has only recently started to be investigated experimentally. We therefore carried out synchrotron X-ray diffraction measurements of an *hcp* Fe-C-Si alloy with 4 at% C and 3 at% Si, up to ~150 GPa. Density functional theory calculations were also performed to examine different incorporation mechanisms. These calculations suggest interstitial C to be more stable than substitutional C below ~350 GPa. In our calculations, we also find that the lowest-energy incorporation mechanism in the investigated pressure range (60–400 GPa) is one where two C atoms occupy one atomic site; however, this is unlikely to be stable at high temperatures. Notably, substitutional C is observed to decrease the volume of the *hcp* Fe, while interstitial C increases it. This allows us to use experimental and theoretical equations of state to show unambiguously that C in the experimental *hcp* Fe-C-Si alloys is not substitutional, as is often assumed. This is crucial since assuming an incorrect incorporation mechanism in experiments leads to incorrect density determinations of ~4%, undermining attempts to estimate the concentration of C in the inner core. In addition, the agreement between our experiments and calculations supports Si and C as being light elements in the inner core.

1. Introduction

The only direct investigation of the inaccessible Earth's deep interior is provided by seismological studies of sound wave velocities through the Earth. The comparison between seismological observations and elastic properties of candidate materials at the relevant conditions present in the deep Earth allows to relate geophysical data with the chemistry and temperature of the Earth's interior. In the Earth's mantle, mineralogical and compositional models can match the observed velocities to approximately 1% (e.g., Bass & Zhang, 2015; Irifune et al., 2008; Kurnosov et al., 2017; Murakami et al., 2012; Pamato et al., 2016). Conversely, for the inner core, sound wave velocities of pure Fe or Fe-Ni alloys in the *hcp* structure usually obtained from mineral physics are much higher (10–30%) than those from seismic observations (Belonoshko et al., 2007; Martorell, Brodholt, et al., 2013; Vočadlo, 2007). Numerous arguments were proposed over the years to explain these discrepancies, including, large compositional effects, pervasive partial melting, anelasticity, or the stabilization of *bcc* Fe (Antonangeli et al., 2004; Belonoshko et al., 2003, 2007, 2017, 2019; Vočadlo, 2007).

Theoretical calculations have shown that the sound velocities observed in the inner core could be matched by *hcp* Fe due to a strong nonlinear softening of the elastic properties at 360 GPa above 7,000 K (Martorell, Vočadlo, et al., 2013). However, even though the velocities of the inner core were matched by pure Fe, the density remained too high (by 2–3%) to agree with geophysical observations, and so lighter elements are still needed to explain this density mismatch. Furthermore, the suggested premelting softening is generally suppressed in iron alloys (e.g., Martorell et al., 2016). With the exception of Fe₇C₃ (Chen et al., 2014; Prescher et al., 2015), all the iron compounds examined so far exhibit higher velocities than those found in the core.

For the case of Fe₇C₃, a strong nonlinear softening has been also observed (Li et al., 2016), but, while the calculated velocities agree with seismic data, the density is far too low (by ~8%). Many recent computational and experimental studies addressing core compositions point to the need of two or more distinct light elements (e.g., Badro et al., 2014; Edmund et al., 2019; Li et al., 2018; Morard, Nakajima, et al., 2017). However, the identity of this light element mixture is still largely debated. Very recently, Li et al. (2018) reported ab initio molecular dynamics (AIMD) calculations, which reveal the observed inner-core density and sound velocities can be simultaneously matched by a range of ternary and quaternary Fe alloys, all containing carbon. This constrains possible solid solution's space in a multiple light elements model explaining all of the major seismic constraints. However, even when limiting the discussion to mineral physics properties, several aspects still remain uncertain, including the different incorporation mechanisms of C in Fe and its effect on seismic properties. From density functional theory (DFT) calculations, Huang et al. (2005) suggested that C takes the substitutional form in *hcp* Fe at 0 K above approximately 300 GPa, as confirmed by Li et al. (2019), who, using AIMD, also found that C takes the substitutional form at 360 GPa and 6,500 K. However, at lower pressures, interstitial C and other complex defect structures may be stabilized (Caracas, 2017; Huang et al., 2005; Li et al., 2019). In fact, the thermodynamic model of Fei and Brosh (2014), based on experiments at pressures <20 GPa, and more recently the work by Yang et al. (2019) indicate that the interstitial form is preferred up to inner-core pressures. The change of incorporation mechanism may be related to the variance of solubility. Lord et al. (2009), for example, found a negligible C solubility in *hcp* Fe approaching 50 GPa. However, more recently, Mashino et al. (2019) performed melting experiments up to 255 GPa and predicted a solubility of 1 wt.% in *hcp* Fe at inner-core boundary conditions. A question remains as to whether different incorporation mechanisms of C in iron have an effect on the seismic properties of an Fe-C alloy; does it matter if the carbon is on an interstitial, substitutional, or other site within the *hcp* crystal structure?

Multiple lines of evidence, from geochemical and cosmochemical arguments (e.g., Allègre et al., 1995), to core formation models based on metal-silicate partitioning (e.g., Fischer et al., 2015; Siebert et al., 2013), to isotopic considerations (e.g., Fitoussi et al., 2009; Shahar et al., 2009), support silicon to be present in the core. Due to the almost equal Si partitioning between liquid and *hcp* iron (Alfè et al., 2002), the quantity of Si present in the inner core is not significantly different from that expected for the liquid core. However, many recent studies point out that Si is very unlikely to be the only light element in the core (Badro et al., 2014; Morard, Andrault, et al., 2017) and specifically in the inner core (Antonangeli et al., 2018; Edmund et al., 2019; Martorell et al., 2016). An alloy in the ternary Fe-C-Si system thus seems to provide the simplest composition possibly accounting for the bulk of geophysical and geochemical evidences of the inner core. In particular, very recent AIMD calculations (Li et al., 2018) indicate that an *hcp* Fe₆₀C₂Si₂ alloy is expected to have density, compressional, and shear sound velocities matching those of PREM at 360 GPa for simulation temperatures between 6,000 and 7,000 K.

To confirm this prediction, both high-pressure experiments and further simulations need to be performed to clarify the effects of C on the seismic properties of Fe and Fe-Si alloys over a wider range of pressures and temperatures. Thus, here we address the effect of the C incorporation mechanism on density by combining synchrotron X-ray diffraction (XRD) measurements on an *hcp* Fe-C-Si alloy (with 4 at% C and 3 at% Si at 300 K and up to ~150 GPa), with DFT calculations. In particular, we examined the different incorporation mechanisms of carbon in the structure of the alloy as a function of pressure. Our results are then used to discuss the density of a Fe-C-Si alloy at inner core conditions.

2. Materials and Methods

2.1. Experiments

The starting material, with a nominal composition of Fe 93 at%, C 4 at%, and Si 3 at%, was synthesized by an ultrarapid quench method at the ICMPE (Institut de Chimie et des Matériaux de Paris-Est, Paris, France) using nominally pure Fe (Neyco F-12734), Si (Wacker), and Fe₃C (Neyco FC-76857/1). Homogeneous Fe alloys, in the form of ribbons, approximately 25 μm thick and of 20–30 mm width, were synthesized following the procedure described in Morard et al. (2011).

The chemical composition of the synthesized alloys was measured by means of a Cameca SX100 electron microprobe analyzer equipped with a cold finger and an O₂ flux at Camparis center-Sorbonne Université. The resulting composition for the alloy is 3 (±0.2) at% Si, 4 (±0.4) at% C, and 93 (±0.06) at% Fe

($\text{Fe}_{93}\text{C}_4\text{Si}_3$). In addition, scanning electron microscopy (SEM) analyses were performed on the sample using a Zeiss Ultra 55 scanning electron microscope installed at the IMPMC (Institut de Minéralogie, de Physique des Matériaux et de Cosmochimie), confirming homogeneity at the micron scale (Miozzi, Morard, et al., 2020).

Samples were prepared for the high-pressure experiments by crushing parts of a ribbon specimen and compressing it between two diamonds ($\sim 600\ \mu\text{m}$ culet), in order to obtain the desired thickness (usually between 5 and 10 microns). The sample was then loaded in a rhenium gasket of $20\ \mu\text{m}$ thickness, with a hole of $60\ \mu\text{m}$, with $100/300\ \mu\text{m}$ beveled anvils. High pressures were generated using a Le Toullec-type (membrane-driven) diamond anvil cell. Tungsten carbide seats designed for diamonds with conical support were used (Boehler & De Hantsetters, 2004). The sample was loaded alongside Mo as a pressure calibrant, with Ne acting as the pressure transmitting medium; the equation of state parameters for the Mo pressure calibrant were taken to be $V_0 = 31.14\ \text{\AA}^3$ (Litasov et al., 2013; Ross & Hume-Rothery, 1963), $K_0 = 260(1)\ \text{GPa}$, and $K' = 4.19(5)$.

Angle-dispersive XRD measurements were carried out at the ID27 beamline of the European Synchrotron Radiation Facility in Grenoble (Mezouar et al., 2005). In the experiments, a monochromatic beam of $33\ \text{keV}$ ($\lambda = 0.3738\ \text{\AA}$) was focused on an area $< 3 \times 3\ \mu\text{m}^2$ (full width at half maximum). Data collection times were typically between 10 and 30 s; diffraction patterns were collected on a MAR CCD detector at pressures between 48 and 150 GPa at 300 K.

Two-dimensional diffraction images were integrated using the software DIOPTAS (Prescher & Prakapenka, 2015), using calibration parameters (sample detector distance and orientation) derived from the diffraction pattern of a cerium dioxide (CeO_2) standard. Diffraction patterns were indexed with PD Indexer (http://pmsl.planet.sci.kobe148u.ac.jp/~seto/?page_id=20). The sample started to transform from the *bcc* structure stable at ambient pressure to the *hcp* structure at $\sim 19\ \text{GPa}$. All *bcc* reflections were absent by $\sim 22\ \text{GPa}$. At least five sample diffraction lines are clearly observed for the *hcp* phase over the entire pressure range. However, the diffraction patterns are, to some extent, nonideal in terms of randomness of the distribution (both 101 and 102 reflections showed intensity variation around the powder ring). Also, the 002 reflection, while present over the entire pressure range, is very weak, due to a small preferential orientation, likely induced by sample thinning before loading. Therefore, it was not possible to perform full profile data refinements. The unit-cell parameters were thus calculated from the *d* spacings of the reflections 100, 101, 102, and 110 using the software Unit Cell by Holland and Redfern (1997).

2.2. DFT Calculations

DFT calculations were performed by using a $4 \times 4 \times 2$ *hcp* supercell, the VASP code (Kresse & Joubert, 1999) and PAW potential (Blöchl, 1994). The valence states $3p^6 3d^6 4s^2$, $3s^2 3p^2$, and $2s^2 2p^2$ were adopted for Fe, Si, and C, respectively. We employed the generalized gradient approximation (GGA); the Perdew-Wang (Perdew & Wang, 1992) exchange-correlation functional was used. We adopted the ordered symmetrical structure for the alloy by placing solid solution atoms with the maximum sum of distances between them to achieve homogeneous dispersion. The octahedral interstitial site was adopted for the interstitial carbon atoms, as the tetrahedral interstitial site was reported to be less favorable (Caracas, 2017). A plane wave cutoff energy of 400 eV and 12 irreducible *k* points were used to converge the results.

3. Results and Discussion

3.1. Equations of State

The diffraction pattern of the investigated alloy collected at 140 GPa (the upper end of the pressure range investigated) and indexed as hexagonal closed packed (*hcp*) iron is shown in Figure 1.

Measured unit-cell volumes of *hcp* $\text{Fe}_{93}\text{C}_4\text{Si}_3$ alloy are presented in Figure 2 and show a smooth, continuous trend with increasing pressure, indicating the absence of any phase transition within the pressure range investigated.

The *P-V* data, reported in Table S1 in the supporting information, were fitted using a third-order Birch-Murnaghan equation of state (BM3 EoS; Birch, 1947) with the software EosFit7 (Angel et al., 2014). All the parameters were refined resulting in the following EoS parameters: $V_0 = 22.7(2)\ \text{\AA}^3$, $K_0 = 148(18)\ \text{GPa}$, and $K_0' = 5.8(4)$ (Table 1). The EoS parameters are usually defined at 0 GPa (e.g., V_0 , K_0 , and K_0').

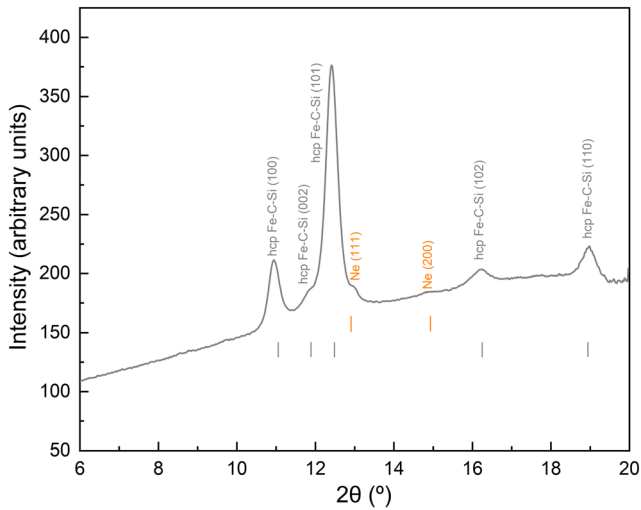


Figure 1. Angle-dispersive X-ray powder diffraction pattern of *hcp* Fe-C-Si alloy (+Ne) collected at ~140 GPa and 300 K. The reflection positions of neon (orange) and Fe-C-Si alloy (gray) are shown by the tick markers.

However, as iron alloys in the *hcp* structure are not stable and cannot be quenched at room pressure and temperature, the EoS parameters can be defined at any other pressure in order to compare different EoS in the pressure stability field of *hcp* phases. The parameters refined relative to a pressure scale from 50 GPa are $V_{P=50} = 18.80(1) \text{ \AA}^3$, $K_{P=50} = 394(6) \text{ GPa}$, and $K'_{P=50} = 4.8(2)$.

The measured unit-cell volumes of $\text{Fe}_{93}\text{C}_4\text{Si}_3$ are larger than those of pure *hcp* Fe, Fe-Si, and Fe-C alloys reported in the literature (Figure 2a). If compared to the pure *hcp* Fe EoS as determined by Dewaele et al. (2006), the P - V trend established here shows a different curvature, with the difference in the volumes increasing at high pressure, thus highlighting a difference in compressibility. On the other hand, differences are less pronounced when compared to recent EoS of pure *hcp* Fe reported by Sakai et al. (2014), Yang et al. (2019), and Miozzi, Matas, et al. (2020). Specifically, the new data on the $\text{Fe}_{93}\text{C}_4\text{Si}_3$ alloy determined here show a compressibility curve comparable to the more recent results for pure *hcp* Fe, but with higher volumes.

3.2. Comparison of Fe-C-Si Alloys

A comprehensive comparison of the equations of state parameters K_0 and K_0' of the different alloys considered here is illustrated in the inset in Figure 2a. The data published by Dewaele et al. (2006), Sakai et al. (2014), Yang et al. (2019), and Miozzi, Matas, et al. (2020) for pure Fe and by Edmund et al. (2019) and Yang et al. (2019) for Fe-Si and Fe-C alloys, respectively, were reevaluated in order to obtain the variance-covariance matrixes (Angel, 2000) and to construct the confidence ellipses (Table 1; inset Figure 2a). The confidence ellipses of our data set are larger than those reported in the literature. This might be due to the different pressure and volume uncertainties, how these are taken into account in the analysis, and to the number and range of measured pressure points in the different studies. Here, both pressure and volume uncertainties were weighted, whereas most of the

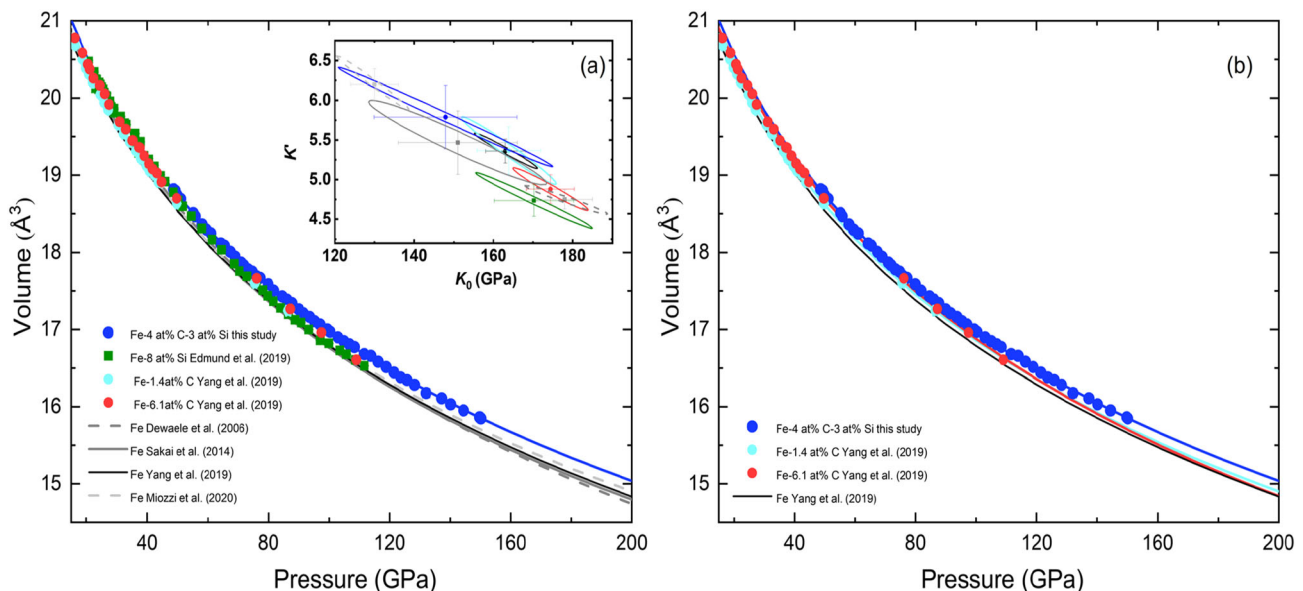


Figure 2. (a) Unit-cell volume of Fe-C-Si alloy as a function of pressure. Error bars are smaller than symbols. Lines correspond to the fit of the data to a third-order Birch-Murnaghan equation of state. Literature data for Fe alloys (Edmund et al., 2019; Yang et al., 2019) and reference EoS for pure Fe (Dewaele et al., 2006; Miozzi, Matas, et al., 2020; Sakai et al., 2014; Yang et al., 2019) are shown for comparison. Inset: confidence ellipses centered on each data point, representing the 68.3% confidence level. The reported 1σ error bars for K_0 and K_0' were derived from least squares refinements. (b) Unit-cell volumes of Fe-C alloys showing effect of C in the unit cell volume of *hcp* Fe.

Table 1
EoS Parameters of *hcp* Fe Alloys

V_0 (Å ³)	K_0 (GPa)	K'	Composition	Reference
Experiments				
22.7(2)	148(18)	5.8(4)	Fe-4 at% C-3 at% Si	This study
22.524(62)	172.4(6.0)	4.64(14)	Fe-8 at% Si	Edmund et al. (2019)
22.5(1)	170(10)	4.7(2)	Fe-8 at% Si	Edmund et al. (2019) (our fit)
22.37(4)	168.9(4.8)	5.18(14)	Fe-1.4 at% C	Yang et al. (2019)
22.40(6)	164(8)	5.4(3)	Fe-1.4 at% C	Yang et al. (2019) (our fit)
22.37(6)	182.2(4.2)	4.68(17)	Fe-6.1 at% C	Yang et al. (2019)
22.44(5)	174(6)	4.88(18)	Fe-6.1 at% C	Yang et al. (2019) (our fit)
22.26(6)	169.7(5.2)	5.19(16)	Fe	Yang et al. (2019)
22.32(5)	163(5)	5.36(5)	Fe	Yang et al. (2019) (our fit)
22.468(24)	165(fixed)	4.97(4)	Fe	Dewaele et al. (2006)
22.31(8)	178(7)	4.75(12)	Fe	Dewaele et al. (2006) (our fit)
22.80(2)	129(6)	6.2(2)	Fe	Miozzi, Matas, et al. (2020)
22.80(7)	130(6)	6.2(2)	Fe	Miozzi, Matas, et al. (2020) (our fit)
22.468(fixed)	155.3(2.2)	5.37(14)	Fe	Sakai et al. (2014)
22.5(2)	151(15)	5.5(4)	Fe	Sakai et al. (2014) (our fit)
Calculations				
20.40	281	4.4	Fe ₆₀ C ₂ ^s Si ₂	This study
20.85	305	4.3	Fe ₆₂ C ₂ ⁱ Si ₂	This study
20.39	313	4.3	Fe ₆₁ C ₂ ^d Si ₂	This study
21.46	291	4.34	Fe-6 at% C ⁱ	Huang et al. (2005)
20.29	312	4.3	Fe	This study

Note. Superscripted “s” = substitutional C; superscripted “i” = interstitial C; superscripted “d” = dimer C.

studies from the literature report an equally weighted fit. When performing an equally weighted fit, errors are smaller, and thus, also, the correlation between K_0 and K_0' is smaller. In addition, given the trade-off between V_0 , K_0 , and K_0' , it is important to measure the volume of the *hcp* structure at the lowest pressure in order to constrain the refinement of the room temperature EoS (see, e.g., Miozzi, Matas, et al., 2020). In our study, due to the lack of low-pressure points (we report P - V data from 48 GPa; see Table S1), the EoS refinement provides a less robust constraint of the reference volume at $P = 0$ (i.e., V_0).

The ellipse representing our data and the one of Yang et al. (2019) for pure Fe intersect at the 68.3% confidence level. Our data are also in good agreement with the recent EoS of Fe reported by Miozzi, Matas, et al. (2020), which extends the data set to lower pressures, and also, within experimental error, with that of Sakai et al. (2014). The confidence ellipses are in fact parallel, and the error bars intersect. All this indicates that the value of the isothermal room pressure bulk modulus obtained in this study for Fe₉₃C₄Si₃ is very similar to the values obtained for pure Fe from Sakai et al. (2014), Yang et al. (2019), and Miozzi, Matas, et al. (2020). A critical review of the EoS parameters of pure Fe is beyond the aim of this paper. It is important to note, however, that the confidence ellipse built with the K_0 and K_0' values of Miozzi, Matas, et al. (2020) intersects only with that of Sakai et al. (2014) for pure Fe, while that of Dewaele et al. (2006) does not intersect with our results and also does not intersect with other results in the literature for pure Fe, as a direct consequence of the different compressibility already mentioned.

Edmund et al. (2019) recently suggested that *hcp* Fe can contain up to 5 wt% Si (approximately 8 at%) without any significant change of the unit cell volume (Figure 2a). As shown by both compression curve and the confidence ellipses, in fact, the data by Edmund et al. (2019) are in good agreement with the data from Dewaele et al. (2006) for *hcp* Fe. Yang et al. (2019) reported that the incorporation of C has a direct effect on the volume of *hcp* Fe. In particular, their fitting results showed that addition of C to Fe leads to larger unit cell volumes at the same pressure, with the magnitude of the increase remaining constant up to ~135 GPa, the highest investigated pressure, with compression curves almost parallel. The authors fitted a BM3 EoS with K_0' fixed to 4.79 (value taken from Fei et al., 2016, for pure Fe) to systematically compare the EoS parameters for pure Fe, Fe-0.31 wt% C (~1.4 at% C) and Fe-1.37 wt% C (~6.1 at% C). However, when the data of Yang et al. (2019) are fitted without constraining K_0' , the resulting magnitude of the volume increase is not the same. Furthermore, it can be seen that extrapolation of the EoS established for Fe-6.1 at% C and Fe-1.4 at% C

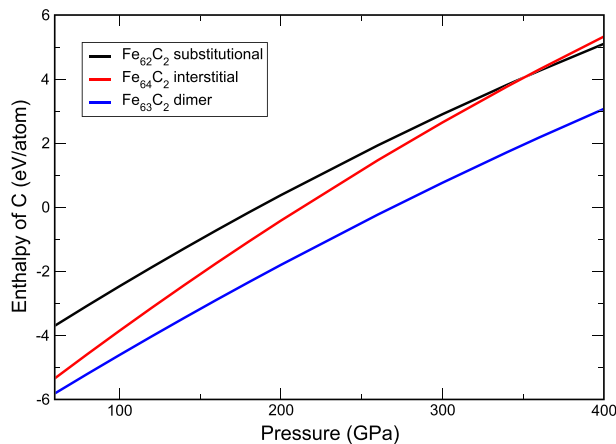


Figure 3. Calculated enthalpy of carbon (referenced to the isolated atom) in the form of substitutional, interstitial, and dimer defects in the *hcp* Fe-C alloy at 0 K.

Impurities, such as C, in a solid can be present as substitutional or interstitial atoms. In addition, impurities can develop defect clusters, possibly modifying the physical and mechanical properties of the material (Li et al., 2017, 2019; Smidt & Sprague, 1972) including its volume and its compressibility. Therefore, it is essential to address the different incorporation mechanisms of carbon in the structure of the alloy at different pressures, to evaluate their relevance in defining the properties of the Earth's core. To this end, in our ab initio calculations, we considered both binary Fe-C and ternary Fe-C-Si alloys. At first we relaxed the structures and calculated enthalpies for the binary substitutional Fe₆₂C₂, interstitial Fe₆₄C₂, and dimer Fe₆₃C₂ (two C at one atomic site) alloys (see the structural illustration in Figure S1). Then, we also calculated volumes and fitted the EoS of pure Fe, Fe₆₀C₂Si₂ via substitution, Fe₆₂C₂Si₂ via interstitial carbon, and Fe₆₁C₂Si₂ with a dimer (Tables S2 and 1, respectively). The composition of the calculated alloys corresponds to Fe ~3 at% C and ~3 at% Si.

Calculations using a 16 Fe atoms supercell (Huang et al., 2005) support a transition from interstitial to substitutional C at pressure of ~300 GPa at 0 K. At high temperature, calculations based on the quasiharmonic approximation (QHA) (Li et al., 2019) showed that the substitutional alloy is more stable than the interstitial one at 360 GPa and 6,500 K, confirming that the temperature effect does not significantly vary the relative stability (at least at inner core pressures). They also showed that the inclusion of C as a dimer is more stable than both substitutional and interstitial alloying at 360 GPa and 0 K but entropy does not favor the dimer and it becomes less stable than substitutional C at 6,500 K (Li et al., 2019). The enthalpies of C in different forms calculated at 0 K in this study are shown as a function of pressure in Figure 3. The enthalpy calculations show that interstitial C is more stable than substitutional C below ~350 GPa. The difference in transition pressure with Huang et al. (2005) may be due to the size effect and concentration dependence. The dimer is shown to be more stable than both the substitutional and interstitial forms at all examined pressures from 60 to 400 GPa. However, on qualitative grounds, considering the temperature effect and entropy cost in forming the dimer, this could become unfavorable at high temperatures. Quantitative high-temperature calculations will be necessary to determine at what temperature the dimer structure becomes unstable, but, in any case, it definitely has its own stability field over a large pressure range extending to a certain temperature. Overall, these theoretical studies show that the interstitial alloy is more stable at low pressures, while the substitutional defect is more stable at 360 GPa. This also implies that a change of C incorporation mechanism is likely under inner-core conditions.

The calculated volumes of the alloys considered, together with those that we measured experimentally, at different pressures are displayed in Figure 4.

Substitutional C decreases the volume of the *hcp* unit cell relative to that of pure Fe, while interstitial C increases it. The dimer also increases the volume of *hcp* Fe but to a much lesser degree than the interstitial defect. Calculated and experimentally determined volumes are in excellent agreement at pressures above ~60 GPa, suggesting that C in the experimental sample is interstitial.

crosses above 120 GPa, with the volumes of the first becoming smaller than the second and approaching the volume of pure Fe (Figure 2b). Even when limiting comparison to the directly investigated pressure range, we note that Fe-6.1 at% C has smaller volumes than the sample studied here, which contains less C (4 at% C), and volumes similar to those of Fe-Si alloy with 8 at% Si (Edmund et al., 2019) and pure Fe by Dewaele et al. (2006). Moreover, as shown in the inset in Figure 2a, the confidence ellipses representing our data and those of Yang et al. (2019) on pure Fe and Fe-1.4 at% C intersect, indicating a shift only in V_0 without changing the compressibility, while that of Fe-6.1 at% C is closer to those of Fe-8 at% Si (Edmund et al., 2019) and pure Fe according to Dewaele et al. (2006).

3.3. Effect of the Incorporation Mechanism of Carbon on the Compressibility of *hcp* Fe

While Si is incorporated via substitution in iron without introducing major changes in the volume (Edmund et al., 2019), the strong effect of small amounts of C on the volume of *hcp* Fe may well be related to its interstitial position in the *hcp* structure (Caracas, 2017; Yang et al., 2019).

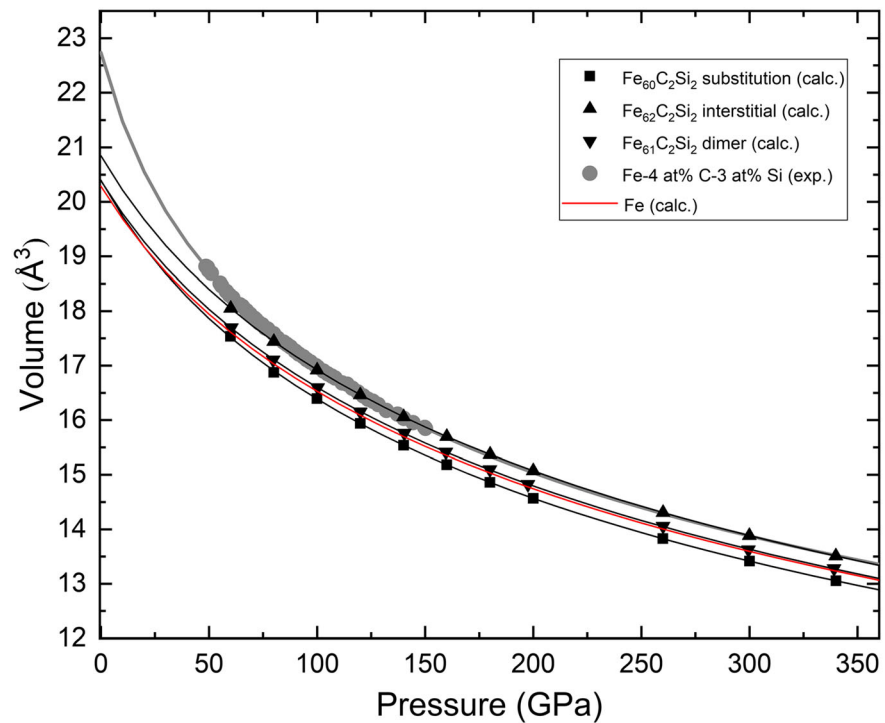


Figure 4. Calculated and measured unit-cell volumes of Fe-C-Si alloys with pressure showing the effect of different incorporation mechanisms of C in the alloy structure. The solid lines are the fit of the data to a third-order Birch-Murnaghan EoS. The red solid line corresponds to the EoS of Fe calculated in this study.

At lower pressures (below 60 GPa) the calculated volumes are smaller than those determined experimentally. This difference is attributed to the approximations in the theoretical approach. DFT may fail to capture the correct electron correlation at low pressures, becoming more reliable at high pressures as a consequence of the increased delocalization of the electrons. This mismatch between calculations and experiments at low pressures has also been observed for *hcp* Fe (Figure 5).

Actually, in the case of pure Fe the difference in volumes is much more pronounced, with the experimental and computational results starting to agree closely only at ~ 200 GPa.

To better understand the effect of C and the incorporation mechanism, Figure 6 shows the pressure dependence of the volume difference $\Delta V = V - V_{\text{Fe}}$ (where V is the unit-cell volume of the alloy and V_{Fe} is the reference unit-cell volume for *hcp* Fe) for *hcp* Fe and Fe-Si-C alloys. The experimental volumes for $\text{Fe}_{93}\text{C}_4\text{Si}_3$ are compared to the different experimental V_{Fe} available in the literature, whereas the calculated volumes are compared to *hcp* Fe from our DFT simulations. Regardless of the reference V_{Fe} used, we can unambiguously confirm that C in the experimental sample is not substitutional as the ΔV for substitutional C is negative. In the pressure range of the experiments (50–150 GPa), the experimental volume differences are close, although slightly higher, to those reported for the dimer configuration, whereas at pressures above 200 GPa, all (except when using the EoS of Miozzi, Matas, et al., 2020) approach the ΔV expected for interstitial C. Once considering the different EoS of *hcp* Fe and the differences among the experiments (pressure scales, hydrostaticity, etc.) and possible problems with the calculations at low pressures, this analysis seems to suggest that C in the experimental sample is interstitial. The more stable dimer might be present in some domains at lower pressures. Possibly the sample synthesis process at ambient pressure and high temperature favored interstitial carbon. Dimer formation in the quenched samples might then be entropically unfavorable or prevented by kinetic barriers and slow diffusion of vacancies.

Previous computational studies (Caracas, 2017; Huang et al., 2005; Li et al., 2019) suggest that C preferentially occupies the octahedral interstitial site at low pressure. The presence of C slightly expands the octahedron containing the impurity, resulting in an increase in unit cell volume (Figures 2 and 4). According to

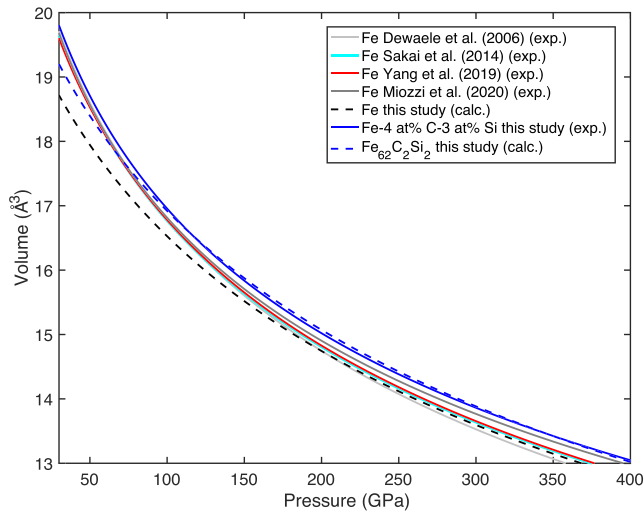


Figure 5. Comparison between calculations and experiments for *hcp* Fe and Fe-C-Si alloys as a function of pressure.

Caracas (2017), the volume increase is almost linear with the amount of C and is approximately independent of pressure within the stability field of the *hcp* phase (see their Figure 2). In agreement with Caracas (2017), the volume increase is almost linear with C content, from 1.4 at% (Yang et al., 2019) to 4 at% C (this study) and almost independent of pressure. Contrarily to the other data sets, Fe-6.1 at% C by Yang et al. (2019) seems not to follow the same trend; above ~80 GPa the volume ratio decreases as a function of pressure and is much lower than that expected on the basis of the other data for lower C contents, and below that calculated by Caracas (2017) for a similar composition (Figure S2). These data by Yang et al. (2019) also disagree with the EoS predicted for a similar composition (Fe-6 at% C) by Huang et al. (2005), and, therefore, it appears that Fe-6.1at% C by Yang et al. (2019) may not be an interstitial solid solution.

To summarize, even a small amount of C in the alloy has a strong effect on the volume of *hcp* Fe. Calculated and experimentally determined volumes are in excellent agreement at pressures above ~60 GPa, suggesting that C in the experimental sample is interstitial. While substitutional C decreases the volume of the *hcp* unit cell, interstitial C increases it. The inclusion of C as a dimer, predicted by calculations to be the most stable, also increases the volume of *hcp* Fe, but to a lesser degree than the interstitial defect.

3.4. Effect of the Incorporation Mechanism of Carbon on the Density

The effect of C on the density of *hcp* Fe is critical to estimation of the effect of C on the physical properties of the Earth's inner core. A common practice in mineral physics is to calculate the density of the alloy assuming a substitutional solid solution, which is valid, for example, for an Fe-Si alloys as Si only enters in the *hcp*

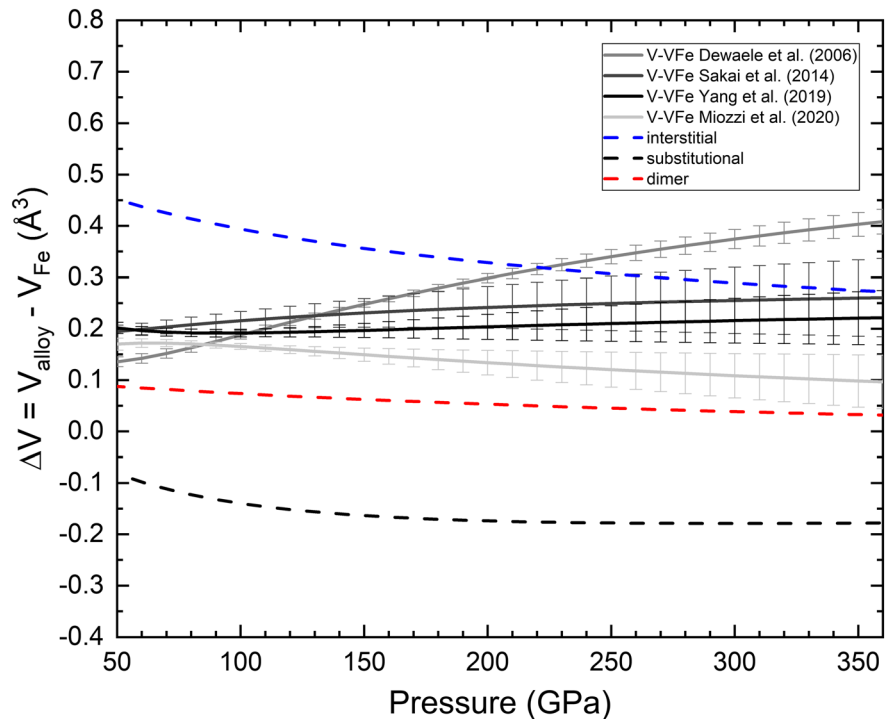


Figure 6. Volume variation, $\Delta V = V - V_{\text{Fe}}$ (where V is the unit-cell volume of the alloy and V_{Fe} is the reference unit-cell volume for *hcp* Fe) for *hcp* Fe alloys as a function of pressure. For the experimental results from the present work, different reference EoS for pure Fe (Dewaele et al., 2006; Miozzi, Matas, et al., 2020; Sakai et al., 2014; Yang et al., 2019) were taken from the literature. The calculated volumes of $\text{Fe}_{62}\text{C}_2\text{Si}_2$ (C interstitial), $\text{Fe}_{61}\text{C}_2\text{Si}_2$ (dimer), and $\text{Fe}_{60}\text{C}_2\text{Si}_2$ (substitutional) are normalized to *hcp* Fe from our DFT simulations.

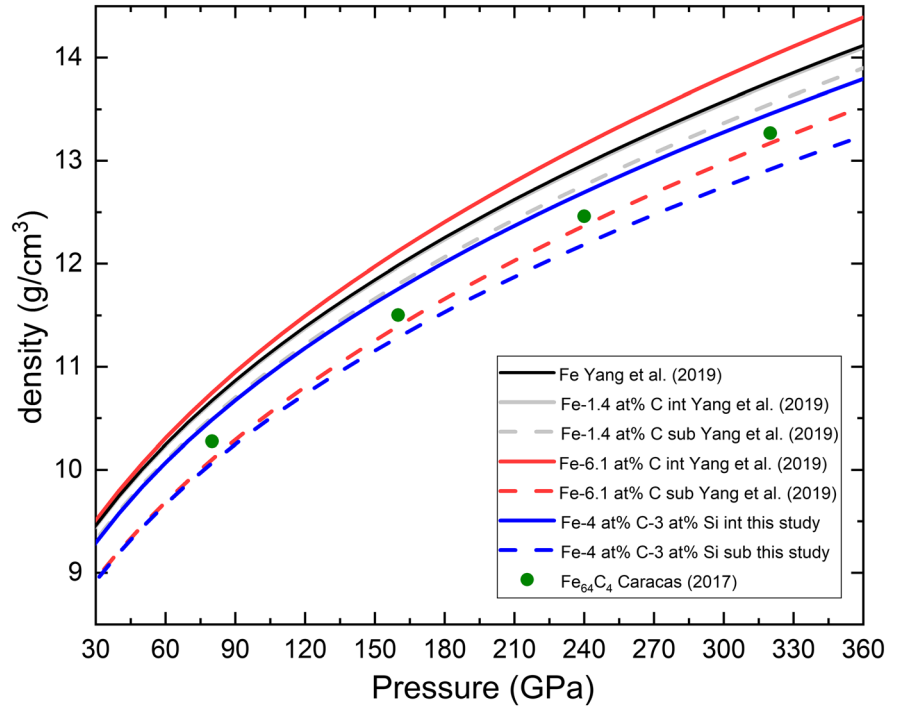


Figure 7. Density evolution with pressure for different *hcp* Fe-C-Si alloys. Solid lines represent densities calculated considering C as interstitial, whereas dashed lines are densities calculated assuming C as substitutional, starting from the same volumes.

structure as a substitutional impurity. In this way, the density of a substitutional alloy $A_{1-x}B_x^s$ (s denotes substitutional) is calculated as follows:

$$\rho = \frac{N \cdot [(1-x) \cdot M_A + x \cdot M_B]}{V}, \quad (1)$$

where N is the number of atoms in unit cell, V is the volume of unit cell, M_A and M_B are the molar mass for A and B , and x is the molar fraction.

However, this is not directly applicable for other alloys like Fe-C, as C can have other solid solution mechanisms, such as incorporation interstitially. Following the established approach for *fcc* Fe-C alloys reported, for example, in Waseda et al. (2011), the density of an interstitial solid solution $A_{1-x}B_x^i$ (i denotes interstitial) in this case is calculated as follows:

$$\rho = \frac{N \cdot \left[M_A + \frac{x}{1-x} M_B \right]}{V}, \quad (2)$$

where the number N of atoms in unit cell in *hcp* Fe is 2 while in *fcc* is 4.

The density in the case of the dimer defect, with two C atoms sitting at one lattice site, can be computed as a combination of one substitutional and one interstitial C.

In this study, the density of Fe-C-Si alloy considering Si as substitutional and C as interstitial $A_{1-x-y}B_x^sC_y^i$ is calculated as follows:

$$\rho = \frac{N \cdot \left[\left(\frac{1-x-y}{1-y} \right) \cdot M_A + \frac{x}{1-y} \cdot M_B + \frac{y}{1-y} M_C \right]}{V}, \quad (3)$$

while if both Si and C are substitutional, the density for $A_{1-x-y}B_x^sC_y^s$ is simply

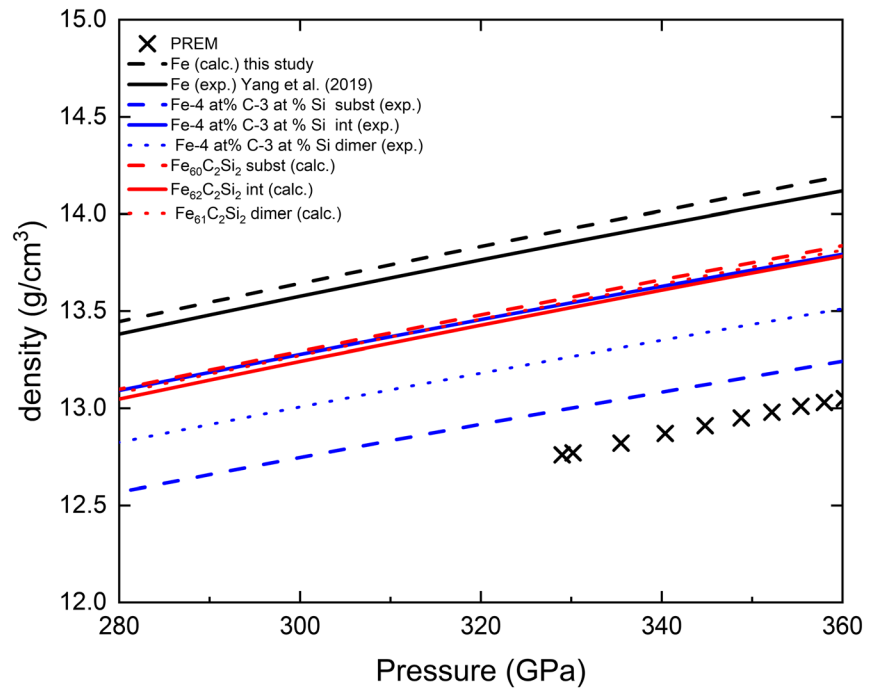


Figure 8. Density variation with pressure for different *hcp* Fe-C-Si alloys calculated at 300 K (experiments) and 0 K (DFT calculations). Dashed lines represent density calculated considering C as substitutional, solid lines are densities calculated assuming C as interstitial, and dotted lines are densities calculated with C as a dimer. For simplicity, only recent data for pure Fe from Yang et al. (2019) are shown as reference. The DFT calculations, in which both the changes in unit-cell volume and unit-cell contents are taken into account in an internally consistent way, show that the density difference between a substitutional, interstitial, and dimer alloy is almost negligible. In the case of the experiments, the volume is directly measured, without any a priori assumption of C distribution and assumptions of effective mass of the unit-cell have to be made to derive density from the measured volumes. If the experimental results are interpreted incorrectly as substitutional, then it would erroneously predict much lower densities.

$$\rho = \frac{N \cdot [(1 - x - y) \cdot M_A + x \cdot M_B + y \cdot M_C]}{V} \quad (4)$$

Further details of density calculations of the Fe-C-Si alloy considering Si as substitutional and C both as interstitial and as substitutional are reported in the supporting information. The derived density evolution for *hcp* Fe-C-Si with pressure is shown in Figure 7.

The density of the alloy experimentally determined in this study, with 4 at% C, is ~6.5% smaller than that of pure Fe when C is assumed to be substitutional, whereas it is only ~2.5% smaller when C is assumed to be interstitial, roughly independent of pressure. Density calculations assuming the interstitial incorporation mechanism are in remarkable agreement with DFT calculations also showing a density reduction with added interstitial C in the Fe structure (Caracas, 2017; Li et al., 2018). Caracas (2017) indicated that 1 wt.% (~4.5 at%) C would decrease *hcp* Fe density by approximately 2.8%.

Yang et al. (2019) reported the density of Fe-1.37 wt % C (~6.1 at% C) to be 5.6% smaller than the of pure *hcp* Fe. These authors state that interstitial C in the *hcp* structure enhanced the density difference between pure Fe and the alloy. However, although the authors clearly assume C as interstitial, the densities they report (see their Figure 2) were calculated assuming substitutional solid solution (see our Figure 7). When the densities are calculated starting from the reported volumes using the equation for interstitial carbon, C, the resulting values are anomalously large, even larger than those of pure Fe (see Figure 7). As already discussed, it appears that the Fe-1.37 wt.% C studied by Yang et al. (2019) might not be an interstitial solid solution.

The correct interpretation of the incorporation mechanism is essential for evaluating the identity and amount of light element(s) in the Earth's core. As reported above, the incorporation mechanism affects both the volume and the mass of the unit cell. Substitutional C lowers the volume of the *hcp* unit cell while the

interstitial and, to a lesser degree, the dimer mechanisms increase it (Figures 4 and 6). At the same time, the interstitial mechanism increases the mass while the substitutional mechanism reduces it. The two effects act to cancel each other out when calculating density. In fact, as shown by our DFT simulations, in which both the changes in unit-cell volume and unit-cell contents are taken into account in an internally consistent way, the density difference between a substitutional, interstitial, and dimer alloy is almost negligible (Figure 8).

This is different in the case of the experiments, in which the volume is directly measured, without any prior assumption of C distribution. However, assumptions of the effective mass of the unit-cell have to be made to derive density from the measured volumes. As illustrated in Figure 8, the way this is done might lead to very different densities with very dissimilar conclusions concerning the amount of light elements required to account for PREM values. In particular, if the volume measured in the experiments is due to an interstitial mechanism but is interpreted as being substitutional, the resulting density will be significantly lower, and a much smaller concentration of light element would be required to match PREM. These results indicate that it is vital to know the exact incorporation mechanism of the alloy and its effect on the elastic properties with changing pressure and temperature, to correctly interpret the properties of the inner core. To this end, the combination of experiments and theoretical studies provide unique capabilities.

4. Conclusions

We have carried out volume and density measurements on an *hcp* Fe-C-Si alloy with 4 at% C and 3 at% Si up to ~150 GPa, using a combination of synchrotron powder diffraction and DFT simulations, carried out at the same pressure conditions, to facilitate interpretation of the experiments and to validate the theoretical approach. In particular *hcp* Fe-C-Si alloys with a different incorporation mechanism—substitutional, interstitial, and dimer—were examined to precisely address the effect of C on the physical properties of the alloy.

Enthalpy calculations suggest that interstitial C is more stable than substitutional C below ~350 GPa. While the dimer, with two C atoms replacing an Fe atom, is more stable than both the interstitial and substitutional C, it is destabilized by temperature, and, at ambient temperature, it can be kinetically inhibited by a diffusion barrier. Indeed, we find that C in the experimentally investigated *hcp* Fe-C-Si alloy sample takes the interstitial form, as supported by the very good agreement at pressure above ~60 GPa between the experimentally determined compression curve and that obtained from calculations for the interstitial alloy. Calculated values for density in the literature are often determined assuming a substitutional solid solution. However, this is not applicable for an interstitial-type solid solution, such as that reported here. Assuming the wrong incorporation mechanism when estimating density from measured volumes can lead to incorrect density determination, resulting in a more enhanced density contrast between the alloy and pure Fe. In turn, this can affect density-velocities systematics (Birch's law) resulting in erroneous interpretation of inner core composition. Finally, the agreement between our experiments and calculations supports previous work (Li et al., 2018), suggesting Si and C combined can account for core densities and velocities.

Data Availability Statement

Data will be available at the repository of University of Padova (<http://researchdata.cab.unipd.it/385/>).

Acknowledgments

The authors thank Jeroen Jacobs (ESRF) for his assistance with the diamond anvil cell preparation. M. G. P. received funding from the European Union's Horizon 2020 research and innovation programme under the Marie Skłodowska-Curie Grant Agreement No. 796755. This project has received funding from Natural Environment Research Council (NERC) (Grant NE/M015181/1 to L. V.) and from the European Research Council (ERC) under the European Union's Horizon 2020 research and innovation programme (Grant Agreement No. 724690 to D. A.).

References

- Alfè, D., Gillan, M. J., & Price, G. D. (2002). Composition and temperature of the Earth's core constrained by combining ab initio calculations and seismic data. *Earth and Planetary Science Letters*, *195*(1–2), 91–98. [https://doi.org/10.1016/S0012-821X\(01\)00568-4](https://doi.org/10.1016/S0012-821X(01)00568-4)
- Allègre, C. J., Poirier, J., Humler, E., & Hofmann, A. W. (1995). The chemical composition of the Earth. *Earth and Planetary Science Letters*, *134*(3–4), 515–526. [https://doi.org/10.1016/0012-821X\(95\)00123-T](https://doi.org/10.1016/0012-821X(95)00123-T)
- Angel, R. J. (2000). Equations of state. *Reviews in Mineralogy and Geochemistry*, *41*(1), 35–59. <https://doi.org/10.2138/rmg.2000.41.2>
- Angel, R. J., Gonzalez-Platas, J., & Alvaro, M. (2014). EosFit7c and a Fortran module (library) for equation of state calculations. *Zeitschrift Fur Kristallographie*, *229*(5), 405–419. <https://doi.org/10.1515/zkri-2013-1711>
- Antonangeli, D., Morard, G., Paolasini, L., Garbarino, G., Murphy, C. A., Edmund, E., et al. (2018). Sound velocities and density measurements of solid *hcp*-Fe and *hcp*-Fe-Si (9 wt.%) alloy at high pressure: Constraints on the Si abundance in the Earth's inner core. *Earth and Planetary Science Letters*, *482*, 446–453. <https://doi.org/10.1016/j.epsl.2017.11.043>
- Antonangeli, D., Occelli, F., Requardt, H., Badro, J., Fiquet, G., & Krisch, M. (2004). Elastic anisotropy in textured *hcp*-iron to 112 GPa from sound wave propagation measurements. *Earth and Planetary Science Letters*, *225*(1–2), 243–251. <https://doi.org/10.1016/j.epsl.2004.06.004>

- Badro, J., Côté, A. S., & Brodholt, J. P. (2014). A seismologically consistent compositional model of Earth's core. *Proceedings of the National Academy of Sciences of the United States of America*, *111*(21), 7542–7545. <https://doi.org/10.1073/pnas.1316708111>
- Bass, J. D., & Zhang, J. S. (2015). Theory and practice: Techniques for measuring high-P-T elasticity. In *Treatise on geophysics* (2nd ed.). <https://doi.org/10.1016/B978-0-444-53802-4.00037-3>
- Belonoshko, A. B., Ahuja, R., & Johansson, B. (2003). Stability of the body-centred-cubic phase of iron in the Earth's inner core. *Nature*, *424*, 1032–1034. <https://doi.org/10.1038/nature01954>
- Belonoshko, A. B., Fu, J., Bryk, T., Simak, S. I., & Mattesini, M. (2019). Low viscosity of the Earth's inner core. *Nature Communications*, *10*(1), 2483. <https://doi.org/10.1038/s41467-019-10346-2>
- Belonoshko, A. B., Lukinov, T., Fu, J., Zhao, J., Davis, S., & Simak, S. I. (2017). Stabilization of body-centred cubic iron under inner-core conditions. *Nature Geoscience*, *10*(4), 312–316. <https://doi.org/10.1038/ngeo2892>
- Belonoshko, A. B., Skorodumova, N. V., Davis, S., Osipov, A. N., Rosengren, A., & Johansson, B. (2007). Origin of the low rigidity of the Earth's inner core. *Science*, *316*(5831), 1603–1605. <https://doi.org/10.1126/science.1141374>
- Birch, F. (1947). Finite elastic strain of cubic crystals. *Physical Review*, *71*(11), 809–824. <https://doi.org/10.1103/PhysRev.71.809>
- Blöchl, P. E. (1994). Projector augmented-wave method. *Physical Review B*, *50*(24), 17,953–17,979. <https://doi.org/10.1103/PhysRevB.50.17953>
- Boehler, R., & De Hantsetters, K. (2004). New anvil designs in diamond-cells. *High Pressure Research*, *24*(3), 391–396. <https://doi.org/10.1080/08957950412331323924>
- Caracas, R. (2017). The influence of carbon on the seismic properties of solid iron. *Geophysical Research Letters*, *44*, 128–134. <https://doi.org/10.1002/2016GL071109>
- Chen, B., Li, Z., Zhang, D., Liu, J., Hu, M. Y., Zhao, J., et al. (2014). Hidden carbon in Earth's inner core revealed by shear softening in dense Fe₇C₃. *Proceedings of the National Academy of Sciences*, *111*(50), 17,755–17,758. <https://doi.org/10.1073/pnas.1411154111>
- Dewaele, A., Loubeyre, P., Occelli, F., Mezouar, M., Dorogokupets, P. I., & Torrent, M. (2006). Quasihydrostatic equation of state of iron above 2 Mbar. *Physical Review Letters*, *97*(21), 29–32. <https://doi.org/10.1103/PhysRevLett.97.215504>
- Edmund, E., Antonangeli, D., Decremps, F., Miozzi, F., Morard, G., Boulard, E., et al. (2019). Velocity-density systematics of Fe-5wt%Si: Constraints on Si content in the Earth's inner core. *Journal of Geophysical Research: Solid Earth*, *124*, 3436–3447. <https://doi.org/10.1029/2018JB016904>
- Fei, Y., & Brosh, E. (2014). Experimental study and thermodynamic calculations of phase relations in the Fe-C system at high pressure. *Earth and Planetary Science Letters*, *408*, 155–162. <https://doi.org/10.1016/j.epsl.2014.09.044>
- Fei, Y., Murphy, C., Shibazaki, Y., Shahar, A., & Huang, H. (2016). Thermal equation of state of hcp-iron: Constraint on the density deficit of Earth's solid inner core. *Geophysical Research Letters*, *43*, 6837–6843. <https://doi.org/10.1002/2016GL069456>
- Fischer, R. A., Nakajima, Y., Campbell, A. J., Frost, D. J., Harries, D., Langenhorst, F., et al. (2015). High pressure metal-silicate partitioning of Ni, Co, V, Cr, Si, and O. *Geochimica et Cosmochimica Acta*, *167*, 177–194. <https://doi.org/10.1016/j.gca.2015.06.026>
- Fitoussi, C., Bourdon, B., Kleine, T., Oberli, F., & Reynolds, B. C. (2009). Si isotope systematics of meteorites and terrestrial peridotites: Implications for Mg/Si fractionation in the solar nebula and for Si in the Earth's core. *Earth and Planetary Science Letters*, *287*(1–2), 77–85. <https://doi.org/10.1016/j.epsl.2009.07.038>
- Holland, T. J. B., & Redfern, S. A. T. (1997). UNITCELL: A nonlinear least-squares program for cell-parameter refinement implementing regression and deletion diagnostics. *Journal of Applied Crystallography*, *30*(1), 84. <https://doi.org/10.1107/S0021889896011673>
- Huang, L., Skorodumova, N. V., Belonoshko, A. B., Johansson, B., & Ahuja, R. (2005). Carbon in iron phases under high pressure. *Geophysical Research Letters*, *32*, L21314. <https://doi.org/10.1029/2005GL024187>
- Irfune, T., Higo, Y., Inoue, T., Kono, Y., Ohfuji, H., & Funakoshi, K. (2008). Sound velocities of majorite garnet and the composition of the mantle transition region. *Nature*, *451*(7180), 814–817. <https://doi.org/10.1038/nature06551>
- Kresse, G., & Joubert, D. (1999). From ultrasoft pseudopotentials to the projector augmented-wave method. *Physical Review B: Condensed Matter and Materials Physics*, *59*(3), 1758–1775. <https://doi.org/10.1103/PhysRevB.59.1758>
- Kurnosov, A., Marquardt, H., Frost, D. J., Ballaran, T. B., & Ziberna, L. (2017). Evidence for a Fe³⁺-rich pyroclitic lower mantle from (Al,Fe)-bearing bridgmanite elasticity data. *Nature*, *543*(7646), 543–546. <https://doi.org/10.1038/nature21390>
- Li, Y., Korzhavyi, P. A., Sandström, R., & Lilja, C. (2017). Impurity effects on the grain boundary cohesion in copper. *PHYSICAL REVIEW MATERIALS*, *1*(R), 70602. <https://doi.org/10.1103/PhysRevMaterials.1.070602>
- Li, Y., Vočadlo, L., Alfè, D., & Brodholt, J. (2019). Carbon partitioning between the Earth's inner and outer core. *Journal of Geophysical Research: Solid Earth*, *124*, 12,812–12,824. <https://doi.org/10.1029/2019JB018789>
- Li, Y., Vočadlo, L., Brodholt, J., & Wood, I. G. (2016). Thermoelasticity of Fe₇C₃ under inner core conditions. *Journal of Geophysical Research: Solid Earth*, *121*, 5828–5837. <https://doi.org/10.1002/2016JB013155>
- Li, Y., Vočadlo, L., & Brodholt, J. P. (2018). The elastic properties of hcp-Fe alloys under the conditions of the Earth's inner core. *Earth and Planetary Science Letters*, *493*, 118–127. <https://doi.org/10.1016/j.epsl.2018.04.013>
- Litasov, K. D., Dorogokupets, P. I., Ohtani, E., Fei, Y., Shatskiy, A., Sharygin, I. S., et al. (2013). Thermal equation of state and thermodynamic properties of molybdenum at high pressures. *Journal of Applied Physics*, *113*(9), 093507. <https://doi.org/10.1063/1.4794127>
- Lord, O. T., Walter, M. J., Dasgupta, R., Walker, D., & Clark, S. M. (2009). Melting in the Fe-C system to 70 GPa. *Earth and Planetary Science Letters*, *284*(1–2), 157–167. <https://doi.org/10.1016/j.epsl.2009.04.017>
- Martorell, B., Brodholt, J., Wood, I. G., & Vočadlo, L. (2013). The effect of nickel on the properties of iron at the conditions of Earth's inner core: Ab initio calculations of seismic wave velocities of Fe-Ni alloys. *Earth and Planetary Science Letters*, *365*, 143–151. <https://doi.org/10.1016/j.epsl.2013.01.007>
- Martorell, B., Vočadlo, L., Brodholt, J., & Wood, I. G. (2013). Strong premelting effect in the elastic properties of hcp-Fe under inner-core conditions. *Science*, *342*(6157), 466–468. <https://doi.org/10.1126/science.1243651>
- Martorell, B., Wood, I. G., Brodholt, J., & Vočadlo, L. (2016). The elastic properties of hcp-Fe_{1-x}Si_x at Earth's inner-core conditions. *Earth and Planetary Science Letters*, *451*, 89–96. <https://doi.org/10.1016/j.epsl.2016.07.018>
- Mashino, I., Miozzi, F., Hirose, K., Morard, G., & Sinmyo, R. (2019). Melting experiments on the Fe-C binary system up to 255 GPa: Constraints on the carbon content in the Earth's core. *Earth and Planetary Science Letters*, *515*, 135–144. <https://doi.org/10.1016/j.epsl.2019.03.020>
- Mezouar, M., Crichton, W. A., Bauchau, S., Thurel, F., Witsch, H., Torrecillas, F., et al. (2005). Development of a new state-of-the-art beamline optimized for monochromatic single-crystal and powder X-ray diffraction under extreme conditions at the ESRF. *Journal of Synchrotron Radiation*, *12*(5), 659–664. <https://doi.org/10.1107/S0909049505023216>
- Miozzi, F., Matas, J., Guignot, N., Badro, J., Siebert, J., & Fiquet, G. (2020). A new reference for the thermal equation of state of iron. *Minerals*, *10*(2). <https://doi.org/10.3390/min10020100>

- Miozzi, F., Morard, G., Antonangeli, D., Baron, M. A., Boccato, S., Pakhomova, A., et al. (2020). Eutectic melting of Fe-3 at% Si-4 at% C up to 200 GPa and implications for the Earth's core. *Earth and Planetary Science Letters*, *544*, 116382. <https://doi.org/10.1016/j.epsl.2020.116382>
- Morard, G., Andraut, D., Antonangeli, D., Nakajima, Y., Auzende, A. L., Boulard, E., et al. (2017). Fe-FeO and Fe-Fe₃C melting relations at Earth's core-mantle boundary conditions: Implications for a volatile-rich or oxygen-rich core. *Earth and Planetary Science Letters*, *473*, 94–103. <https://doi.org/10.1016/j.epsl.2017.05.024>
- Morard, G., Andraut, D., Guignot, N., Siebert, J., Garbarino, G., & Antonangeli, D. (2011). Melting of Fe-Ni-Si and Fe-Ni-S alloys at megabar pressures: Implications for the core-mantle boundary temperature. *Physics and Chemistry of Minerals*, *38*(10), 767–776. <https://doi.org/10.1007/s00269-011-0449-9>
- Morard, G., Nakajima, Y., Andraut, D., Antonangeli, D., Auzende, A. L., Boulard, E., et al. (2017). Structure and density of Fe-C liquid alloys under high pressure. *Journal of Geophysical Research: Solid Earth*, *122*, 7813–7823. <https://doi.org/10.1002/2017JB014779>
- Murakami, M., Ohishi, Y., Hirao, N., & Hirose, K. (2012). A perovskitic lower mantle inferred from high-pressure, high-temperature sound velocity data. *Nature*, *485*(7396), 90–94. <https://doi.org/10.1038/nature11004>
- Pamato, M. G., Kurnosov, A., Boffa Ballaran, T., Frost, D. J., Ziberna, L., Giannini, M., et al. (2016). Single crystal elasticity of majoritic garnets: Stagnant slabs and thermal anomalies at the base of the transition zone. *Earth and Planetary Science Letters*, *451*, 114–124. <https://doi.org/10.1016/j.epsl.2016.07.019>
- Perdew, J. P., & Wang, Y. (1992). Accurate and simple analytic representation of the electron-gas correlation energy. *Physical Review B*, *45*(23), 13,244–13,249. <https://doi.org/10.1103/PhysRevB.45.13244>
- Prescher, C., Dubrovinsky, L., Bykova, E., Kuppenko, I., Glazyrin, K., Kantor, A., et al. (2015). High Poisson's ratio of Earth's inner core explained by carbon alloying. *Nature Geoscience*, *8*(3), 220–223. <https://doi.org/10.1038/ngeo2370>
- Prescher, C., & Prakapenka, V. B. (2015). DIOPTAS: A program for reduction of two-dimensional X-ray diffraction data and data exploration. *High Pressure Research*, *35*(3), 223–230. <https://doi.org/10.1080/08957959.2015.1059835>
- Ross, R. G., & Hume-Rothery, W. (1963). High temperature X-ray metallography. I. A new debye-scherrer camera for use at very high temperatures II. A new parafocusing camera III. Applications to the study of chromium, hafnium, molybdenum, rhodium, ruthenium and tungsten. *Journal of the Less-Common Metals*, *5*(3), 258–270. [https://doi.org/10.1016/0022-5088\(63\)90031-6](https://doi.org/10.1016/0022-5088(63)90031-6)
- Sakai, T., Takahashi, S., Nishitani, N., Mashino, I., Ohtani, E., & Hirao, N. (2014). Equation of state of pure iron and Fe_{0.9}Ni_{0.1} alloy up to 3 Mbar. *Physics of the Earth and Planetary Interiors*, *228*, 114–126. <https://doi.org/10.1016/j.pepi.2013.12.010>
- Shahar, A., Ziegler, K., Young, E. D., Ricolleau, A., Schauble, E. A., & Fei, Y. (2009). Experimentally determined Si isotope fractionation between silicate and Fe metal and implications for Earth's core formation. *Earth and Planetary Science Letters*, *288*(1–2), 228–234. <https://doi.org/10.1016/j.epsl.2009.09.025>
- Siebert, J., Badro, J., Antonangeli, D., & Ryerson, F. J. (2013). Terrestrial accretion under oxidizing conditions. *Science*, *339*(6124), 1194–1197. <https://doi.org/10.1126/science.1227923>
- Smidt, F. A., & Sprague, J. A. (1972). Property changes resulting from impurity-defect interactions in iron and pressure vessel steel alloys. In ASTM Special Technical Publication.
- Vočadlo, L. (2007). Ab initio calculations of the elasticity of iron and iron alloys at inner core conditions: Evidence for a partially molten inner core? *Earth and Planetary Science Letters*, *254*(1–2), 227–232. <https://doi.org/10.1016/j.epsl.2006.09.046>
- Waseda, Y., Matsubara, E., & Shinoda, K. (2011). *X-Ray Diffraction Crystallography*. Berlin Heidelberg: Springer. <https://doi.org/10.1007/978-3-642-16635-8>
- Yang, J., Fei, Y., Hu, X., Greenberg, E., & Prakapenka, V. (2019). Effect of carbon on the volume of solid Iron at high pressure: Implications for carbon substitution in iron structures and carbon content in the Earth's inner core. *Minerals*, *9*(12), 720. <https://doi.org/10.3390/min9120720>